PAN
ARCHIVES OF ACOUSTICS
Vol. **46**, No. 2, pp. 301–311 (2021)
DOI: 10.24425/aoa.2021.136584

Research Paper

Observation and Modelling on the Shipping Noise in Shallow Waters with Complex Islands and Reefs of the East China Sea

Zilong PENG[(1)*], Fulin ZHOU[(2)], Jun FAN[(2)], Bin WANG[(2)], Huabing WEN[(1)]

[(1)] *Institute of Noise and Vibration*
School of Energy and Power Engineering
Jiangsu University of Science and Technology
Zhenjiang 212003, People's Republic of China
[*]Corresponding Author e-mail: zlp_just@sina.com

[(2)] *Collaborative Innovation Center for Advanced Ship and Deep-Sea Exploration*
State Key Laboratory of Ocean Engineering
Shanghai Jiao Tong University
Shanghai 200240, People's Republic of China

(*received December 19, 2019; accepted November 27, 2020*)

The impact of the noise radiated from merchant ships on marine life has become an active area of research. In this paper, a methodology integrating observation at a single location and modelling the whole noise field in shallow waters is presented. Specifically, underwater radiated noise data of opportunistic merchant ships in the waters of Zhoushan Archipelago were collected at least one day in each month from January 2015 to November 2016. The noise data were analyzed and a modified empirical spectral source level (SSL) model of merchant ships was proposed inspired by the RANDI-3 model (Research Ambient Noise Directionality) methodology. Then combining the modified model with the realistic geoacoustic parameters and AIS data of observed merchant ships, the noise mappings in this area were performed with N×2D of Normal Mode calculations, in which the SSL of each ship was estimated using the modified model. The sound propagation at different receiving positions is different due to the shielding effect of islands and bottom topography. The methodology proposed in this paper may provide a reference for modelling shipping noise in shallow waters with islands and reefs.

Keywords: shipping noise; spectral source level; noise mapping; shallow water; merchant ship.

1. Introduction

It is an important research task to evaluate the contribution to marine ambient noise from human activities and describe the long-term trends in ambient noise levels. Vessel noise from a range of different ship types substantially elevated ambient noise levels across the entire recording from 0.025 to 160 kHz at ranges between 60 and 1000 m (Hermannsen *et al.*, 2014).

In the past five years, some collaborative research projects were done to study the anthropogenic noise around the European waters, such as AQUO (Achieve QUieter Oceans) (Audoly, Rizzuto, 2015; Audoly *et al.*, 2017), SONIC (Suppression of Underwater Noise Induced by Cavitation) and MEPC (Marine Environment Protection Fund) (Robinson *et al.*, 2011). The AQUO project contains three topics: the underwater radiated noise sources were modeled, noise mappings in some specific waters were performed, and the influence on the marine life from the anthropogenic noise was researched (Folegot *et al.*, 2015). In project sponsored by SONIC t, the radiated noise of a small research vessel using three hydrophones was measured in the shallow water (Brooker, Humphrey, 2016). This project was aimed to develop a noise mapping tool to investigate the levels of anthropogenic noise for the EU Marine Strategy Framework Directive (MSFD) (Colin *et al.*, 2015).

The noise mapping tool can provide a representation of shipping noise that is both meaningful to policy makers without acoustic background and representative of the phenomena relevant to the environmental

impact. The accuracy of the end result depends on the quality of the source description as well as that of the propagation model used to compute the sources' combined contributions (Colin *et al.*, 2015).

Leissing and Audoly (Leissing *et al.*, 2014) studied the influence of ship radiated noise level directivity on the assessment of underwater noise maps. They found that the horizontal directivity may significantly improve the prediction accuracy in the assessment of the underwater noise maps. As the sound mapping over large areas can be computationally expensive because of the large number of source and large source-receiver separations involved, Sertlek *et al.* (2016) pointed out that the sound speed profile in shallow water has a negligible effect on the end noise maps by studying the shipping noise in Dutch North Sea, which simplifies the computation greatly.

Based on a simple sound transmission model and ship track data, Erbe *et al.* (2012) mapped the cumulative shipping noise energy throughout 2008 in the west Canadian Exclusive Economic Zone, showing high noise levels in the critical habitats for endangered southern resident killer whales, exceeding limits of "good conservation status" under the EU Marine Strategy Framework Directive. In December 2014, Soares *et al.* (2015) made a prediction on the shipping noise in Portuguese waters, according to the ship track data, and the prediction result was verified by the measurement. Recently, Mustonen *et al.* (2019) made a large-scale and long-term underwater sound monitoring in the Baltic Sea, and the sound was monitored in 36 locations. They concluded that maritime traffic elevates the ambient sound levels in many areas of the Baltic Sea during extensive time periods.

As recommended by the ANSI S12.64 standard (ANSI/ASA, 2009), three hydrophones should be placed at the depths corresponding to target depression angles of 15°, 30°, and 45°. However, for the East China Sea, most areas are in shallow waters. Thus, our acoustic observatory was chosen to be deployed in the busy shipping lane of Shanghai Port. In this study, we analyzed the shipping noise measured in the area of Zhoushan Archipelago with an opportunistic bottom-mounted acoustic observatory, collecting data continuously at least one day in each month from January 2015 to November 2016 (Peng *et al.*, 2018). Although the measurement was very time-consuming and the amount of collected data was huge, the effective shipping noise data were limited to only 57 selected merchant ships (Peng *et al.*, 2018). Then based on the new empirical SSL model, we predicted the noise mapping in this area. This paper is organized as follows. In Sec. 2, we present the measured mean SSL and fitting equations. Inspired by the RANDI-3 model, a modified SSL model was proposed by numerical optimization. In Sec. 3, we present the shipping noise prediction procedure. With the modified model and the geoacoustic environment parameters, we predicted the noise field produced by shipping noise sources. Finally, a summary and a discussion of the results are presented in Sec. 4.

2. Empirical source level model

Our measurements were started in January 2015 and continued until November 2016.The opportunistic transiting ships can be categorized as merchant ship, tanker, fishing vessel and others. Among these ship-types, the largest component is a merchant ship (Peng *et al.*, 2018).

As mentioned in (Simard *et al.*, 2016), the SSL should be estimated when the following criteria are respected: (a) no other ship was present within a radius of 5 km while the focal ship was within the data processing window centered at CPA; (b) the ship speed over ground (SOG) was faster than 1 kn; (c) the d_{CPA} exceeded 100 m.

Furthermore, for estimating the SSL of the focal ship more accurately, the signal-to-noise ratio (SNR) must be greater than 10 dB (Peng *et al.*, 2018). Conforming to the above criteria, we picked the radiated noise data of 57 merchant ships from the large amount of noise data generated by transiting ships, as shown in Table 1. The speeds and lengths of the selected merchant ships are between 6~13.8 kn and 72~200 m, respectively.

During the measurements, for isolating the measured focal ship from others, we had to guarantee the signal-to-noise ratio (SNR), which depends on the background noise and is always present. If the difference is between 3 dB and 10 dB, a correction is made on the measured data.

Based on these criteria, we picked the effective radiated noise data of 57 merchant ships from the large amount of noise data generated by transiting ships. The SLs of the transiting ships are estimated from the received level (RL) at a distant range (r), as shown in Fig. 1, which is compensated for the TL as follows:

$$\mathrm{SL}(f) = \mathrm{RL}(f, r) + \mathrm{TL}(f, r), \tag{1}$$

where f is the frequency [Hz], and r is the slant range along the propagation path [m].

The TLs are calculated with Normal Modes using Kraken, and the geoacoustic parameters and sound speed profile are taken from measured results. The closet distance for each focal ship is chosen from the AIS data (Peng *et al.*, 2018).

From Table 1, SLs of two merchant ships (MMSI: 412378670 and 412499000) are selected to analyze. Their SLs are predicted using several empirical models (Urick model, Ross model, W&H model, and RANDI-3 model) for comparison. As illustrated in Fig. 1, even for the same ship, the predictions with Ross model,

Table 1. Information of selected merchant ships.

MMSI	Ship length	Speed (kt)	CPA [m]	Present Time	Ship type
413249880	98	12	371.6	Jan., 2015	bulk cargo ship
413503780	97	9.7	208.4	Jan., 2015	bulk cargo ship
413552870	96	10.6	343	Jan., 2015	cargo ship
413501150	93	9.3	1046.6	Jan., 2015	multipurpose cargo ship
412378670	173	9.1	806.7	Jan., 2015	bulk cargo ship
413506080	97	10.1	121	Jan., 2015	bulk cargo ship
413436580	180	8.8	725.7	Feb., 2015	bulk cargo ship
412407680	190	13.1	637.4	Feb., 2015	bulk cargo ship
412402070	97	6.9	399.3	Feb., 2015	bulk cargo ship
372748000	140	13.8	617.7	Feb., 2015	container vessel
412422190	114	10.3	1165.6	Feb, 2015	cargo ship
413794000	140	9.1	855.3	Mar., 2015	bulk cargo ship
413377030	159	8.5	935	Mar., 2015	bulk cargo ship
413875000	160	11.8	1287.2	Mar., 2015	bulk cargo ship
412501620	97	10.1	858.7	Mar., 2015	bulk cargo ship
413675000	147	9.3	585.6	Mar., 2015	bulk cargo ship
412750240	134	8.3	777.6	Mar., 2015	bulk cargo ship
413302490	178	8.6	1109.1	Mar.,2015	cargo ship
413301990	95	9.1	432.3	Apr., 2015	cargo ship
412438850	186	11.3	579.3	Apr., 2015	bulk cargo ship
412499000	136	7.5	1122.6	Apr., 2015	container vessel
413409640	97	7.8	1318.9	Apr., 2015	bulk cargo ship
412417210	72	6.5	1067.6	Apr., 2015	cargo ship
412079240	187	11.8	1153.5	May., 2015	bulk cargo ship
413551270	99	10.8	1211	May., 2015	bulk cargo ship
413796000	141	7	906.1	May., 2015	bulk cargo ship
412354220	96	6.5	661.2	May., 2015	cargo ship
413373510	153	9.8	1149.8	May., 2015	bulk cargo ship
413801447	112	6	781.1	May., 2015	bulk cargo ship
412703540	133	9.6	396.5	May., 2015	container vessel
413432110	98	7.3	1217.6	Jun., 2015	bulk cargo ship
412701140	98	10.5	295.3	Jun., 2015	container vessel
413366480	97	8.6	755.2	Jun., 2015	bulk cargo ship
413502420	98	9.6	692.2	Jun., 2015	bulk cargo ship
412271410	90	8.6	504.4	Jun., 2015	dry cargo carrier
412418390	97	9.5	217.3	Jul., 2015	bulk cargo ship
413839000	155	11.3	521.6	Jul., 2015	bulk cargo ship
413503050	96	8.8	662.5	Jul., 2015	cargo ship
413407080	98	7	513.1	Jul., 2015	dry cargo carrier
999955868	98	9.3	682.1	Jul., 2015	cargo ship
413524360	140	7.7	407.1	Jul., 2015	container vessel
413365710	97	9.7	655.8	Aug., 2015	container vessel
412379710	180	13.5	561.1	Nov., 2015	container vessel
100000000	100	7.5	214.5	Nov., 2015	cargo ship
413272050	190	7.9	349.2	Nov., 2015	bulk cargo ship
413500170	98	12	274.3	Apr., 2016	cargo ship
209205000	130	12.8	1296.2	Apr., 2016	container vessel
413329570	106	9.8	607.8	May., 2016	cargo ship
413667000	141	8.3	1304.5	Jun., 2016	cargo ship
412471020	124	11.3	523.3	Aug., 2016	cargo ship
413322830	97	11.1	255.4	Aug., 2016	bulk cargo ship
414709000	200	13.1	766.1	Aug., 2016	bulk cargo ship
413200640	97	9.6	172.3	Aug., 2016	bulk cargo ship
312524000	76	6.8	474.6	Aug., 2016	bulk cargo ship
413352250	129	10	525.8	Aug., 2016	bulk cargo ship
413699220	147	9.6	392.7	Aug., 2016	bulk cargo ship
413371280	94	12.3	865.7	Aug., 2016	container vessel

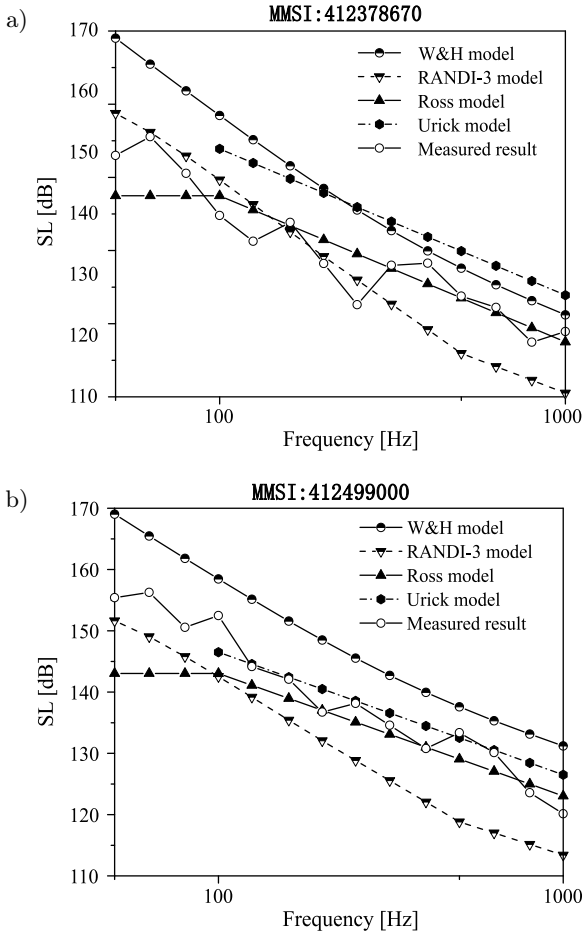

Fig. 1. Comparisons between estimations and measurements of selected ships.

W&H model and Urick model are different (the maximum difference is ~20 dB), not to mention how consistent are these predictions with the measured results. Measured SLs above 100 Hz decreased approximately with $-N \lg f$, and N is about 16.6~32.5. But for the frequencies below 100 Hz, the frequency dependency of source level is not monotonous and relatively complicated. In general, there is a significant hump whose shape, position and level will be influenced by the shipping speed. Although the trends of the measured results above 100 Hz are basically consistent with those of the empirical models, there is still a great gap in levels.

For the results below 100 Hz, the lowest frequency is considered as 50 Hz. Due to the fact that our measured works were made in shallow water, the cut-off frequency can lead to low frequency filtration, and lower frequency noise cannot propagate to far field normally. The cut-off frequency, for the condition bottom is not absolute hard, can be estimated using the following formula from the classical textbook "Principles of Underwater Sound":

$$f_0 = \frac{c_1}{4h}\sqrt{\frac{1}{1-(c_1/c_2)^2}}, \tag{2}$$

where c_1 and c_2 are the sound speed of seawater and the bottom, respectively. h is the local depth.

As illustrated in Fig. 2 and Table 2, considering the Comp. speed with 1549 m/s of the sea floor, a layer of clayey silt with 35 cm thickness, is closer to the sound speed with 1520 m/s than that of fine sand subbottom with 1749 m/s. c_2 is thus set to be 1749 m/s. The cut-off frequency can be easily obtained as 31.5 Hz.

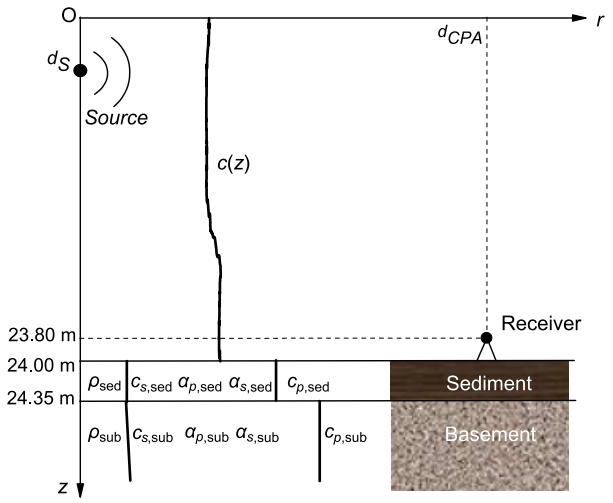

Fig. 2. The sketch of sound propagation with real bottom.

Table 2. Parameter description of bottom.

Description	Symbol	Value
Sediment: clayey silt		
Comp. speed [m/s]	$c_{p,\mathrm{sed}}$	1549
Comp. attenuation [dB/λ_p]	$\alpha_{p,\mathrm{sed}}$	0.6
Shear wave speed [m/s]	$c_{s,\mathrm{sed}}$	80
Shear attenuation [dB/λ_s]	$\alpha_{s,\mathrm{sed}}$	1.25
Density [g/cm^3]	ρ_{sed}	1.488
Subbottom: fine sand		
Comp. speed [m/s]	$c_{p,\mathrm{sub}}$	1749
Comp. attenuation [dB/λ_p]	$\alpha_{p,\mathrm{sub}}$	0.8
Shear wave speed [m/s]	$c_{s,\mathrm{sub}}$	80
Shear attenuation [dB/λ_s]	$\alpha_{s,\mathrm{sub}}$	2.5
Density [g/cm^3]	ρ_{sub}	1.941

However, the cut-off frequency is estimated not accurately enough from the formula. It is necessary to calculate the sound propagation according to the real type of bottom. The sound contour from a point source with the depth of 4 m using 2D axisymmetric finite element method (FEM), as shown in Fig. 3. The sound contour for 30 Hz presents an abnormal propagation close to exponential attenuation. For the frequencies above 50 Hz, the propagation is relatively effective.

The geoacoustic parameters (Jensen *et al.*, 2000; Hamilton, 1980) are described in Table 2, and the ocean empirical sound speeds in this area are shown in

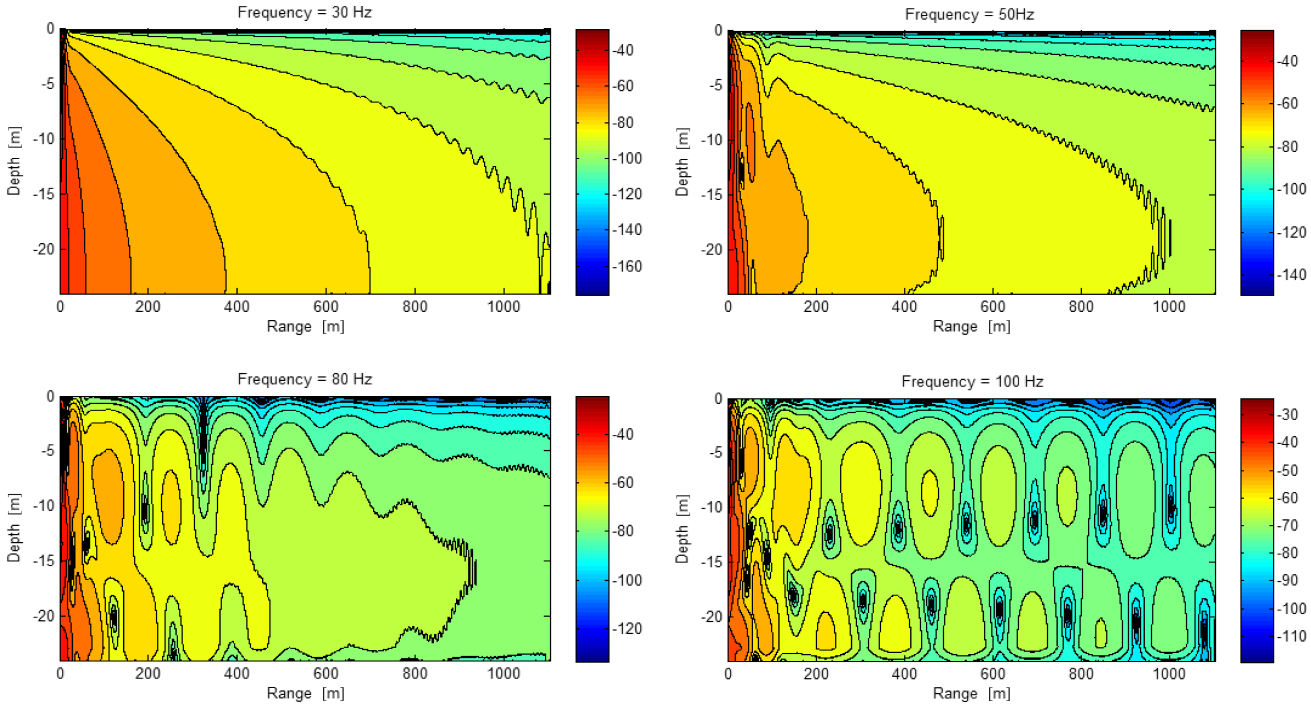

Fig. 3. The transmission loss contour with the depth of 4 m using FEM.

Fig. 4a for different months (Chen, 1992). A sound-speed profile measured on June 7, 2017 is shown in Fig. 4b.

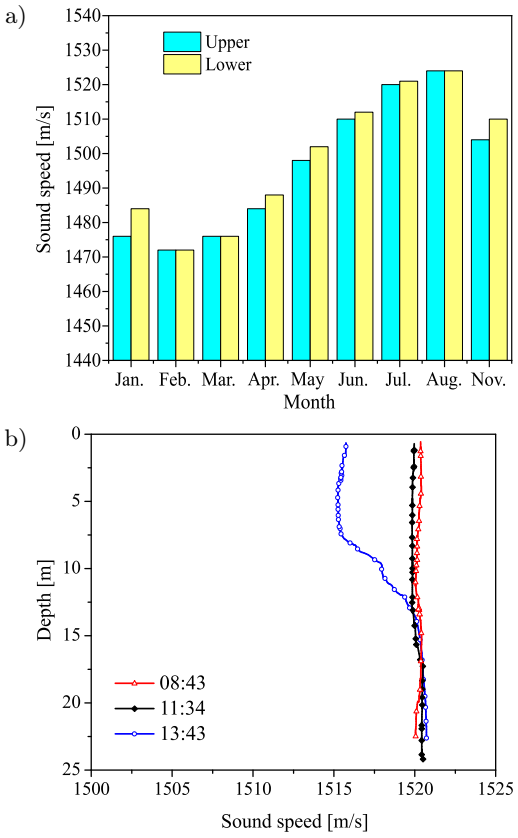

Fig. 4. The sound-speed profile *in situ* measured on June 7, 2017 (a, b).

From the measured results as shown in Fig. 5, some important regularities and information can be obtained: decay slopes with frequency of source levels depend on ship speed or ship length, and the "average" ship's source level. Among them, the "average" ship's source level is the key component, which not only gives the SSL basic skeleton of measured merchant ships, but also contains the dependent information about frequency. It is conceivable that "average" ship's source level will be different if the group constitutions (including length, speed and ship type) are quite different. If the number of samples is sufficiently large, the "average" ship's source level tends to be stable and has more universal meaning.

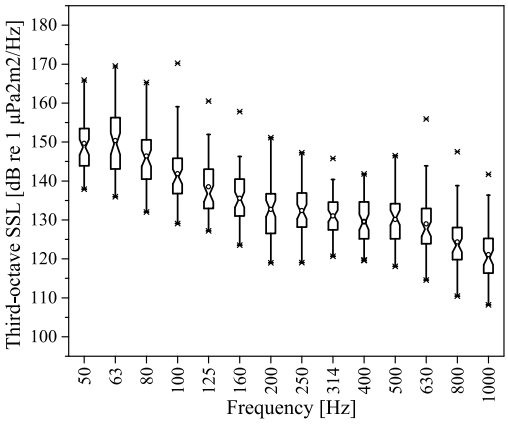

Fig. 5. Measured SSLs of 57 merchant ships.

Here, the "average" ship can be defined as one with a speed of 9.6 kn and a length of 124 m. It should

be noted that the "average" ship's SSLs are obtained from the 57 selected merchant ships. Inspired by the methodology of the RANDI-3 model, we firstly give the "average" ship's source level obtained from the mean curve according to the equation as follows:

$$L_{s,\mathrm{mean}} = 10\lg\left(\frac{1}{N}\sum_{i=1}^{N}10^{L_{s,i}/10}\right), \tag{3}$$

where $L_{s,i}$ is the SSLs of the i-th ship, and $L_{s,\mathrm{mean}}$ is the averaged SSLs of the N ships.

By fitting the measured mean SSLs, we obtained the "average" ship's SSLs L_{so} dependence on frequency in third-octave bandwidths as follows:

$$L_{so} = -10\lg\left(10^{-3.97\lg f-9.00} + 10^{4.23\lg f-23.64}\right). \tag{4}$$

The correlation coefficient R-square is 0.967. The 95% confidence bounds at frequencies from 50 Hz to 200 Hz in third octave bands are shown in Fig. 6.

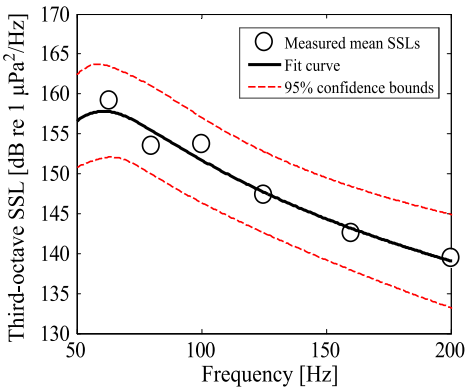

Fig. 6. Variation in average SSL *vs* frequency, the curve is the regression analysis to the entire data set.

The source level can be divided into 4 components as follows:

$$L_s(f,v,l) = L_{so}(f) + K\lg\left(\frac{v}{v_0}\right) + 18\lg\left(\frac{l}{l_0}\right) + L_{\mathrm{res}}, \tag{5}$$

where L_{so} is given by Eq. (4), K is taken as 38 below 100 Hz and 49 above 100 Hz, respectively (Peng *et al.*, 2018); l and v are ship length and speed, respectively; l_0, and v_0 are the ship length and speed of defined "average" vessel, respectively. The last term L_{res} can be described as follows (Breeding *et al.*, 1996):

$$L_{\mathrm{res}} = (k_1 + k_2\lg f)l^{k_3} + k_4, \tag{6}$$

where k_1, k_2, k_3, and k_4 are the undetermined coefficients.

Thus, the numerical process can be written as follows: finding the unknown coefficients and such as the target function below is minimized,

$$\sum_{m=1}^{M}\sum_{q=1}^{Q}\left|L_{\mathrm{res}}^{\mathrm{test}}(f_q,l_m) - \left[(k_1 + k_2\lg f_q)\,l_m^{k_3} + k_4\right]\right|^2, \tag{7}$$

where m and q are the sequence of length and center frequency in 1/3 octave band. f_q is the q-th center frequency in 1/3 octave band, and l_m is the m-th ship length. $L_{\mathrm{res}}^{\mathrm{test}}$ is obtained by subtracting the "average" level L_{so} and terms about speed and length.

According to Eq. (7), we obtained the expression of last term via numerical optimization as follows:

$$L_{\mathrm{res}} = (2.4 + 1.64\lg f)l^{0.063} - 1.3. \tag{8}$$

Finally, we obtained a modified SSL model of merchant ships as follows:

$$\begin{aligned} L_s(f,v,l) &= L_{so}(f) + K\lg\left(\frac{v}{v_0}\right) + 18\lg\left(\frac{l}{l_0}\right) + L_{\mathrm{res}},\\ L_{so}(f) &= -10\lg\left(10^{-3.97\lg f-9.0} + 10^{4.23\lg f-23.64}\right),\\ K &= \begin{cases} 38, & 50\ \mathrm{Hz} \le f < 100\ \mathrm{Hz},\\ 49, & 100\ \mathrm{Hz} \le f \le 200\ \mathrm{Hz}, \end{cases}\\ L_{\mathrm{res}} &= (2.4 + 1.64\lg f)l^{0.063} - 1.3, \end{aligned} \tag{9}$$

where $v_0 = 9.6$ kn, $l_0 = 124$ m. Note that as the average speed and length in modelling are different from those of RANDI-3, the "average" ship with different speeds and lengths is defined as in our work. The range of frequency f [Hz] is only limited from 50 Hz to 200 Hz in third-octave bands. The SSLs of merchant ships at other frequencies are recommended to be estimated by RANDI-3 model.

Furthermore, we analyzed and compared the estimation error (estimation minus measured SSLs) of RANDI-3 model and modified SSL model at 50~200 Hz in third-octaves. The SSL estimations of 57 merchant ships with modified model are shown in Fig. 7a. The prominent "hump" is present at 63 Hz. The Fig. 7b shows the comparison of estimation error with RANDI-3 and the modified model.

As indicated in Fig. 7b, the medians of the estimation error using this modified model with 0.89~3.49 are less than that using RANDI-3 model with 3.98~7.40 over the entire band. In spite of this, the largest interquartile ranges using the modified model (11.67 at 63 Hz) and RANDI-3 model (12.68 at 80 Hz) are still relatively large.

Some reasons below might give a satisfactory explanation:

a) the calculated TL may be inaccurate due to errors in geoacoustic model parameters;

b) the large number of tonal components generated from machinery and propeller contribute to the SSL below 100 Hz which makes the characteristics more complex than those above 100 Hz;

c) the number of measured merchant ships is still not enough;

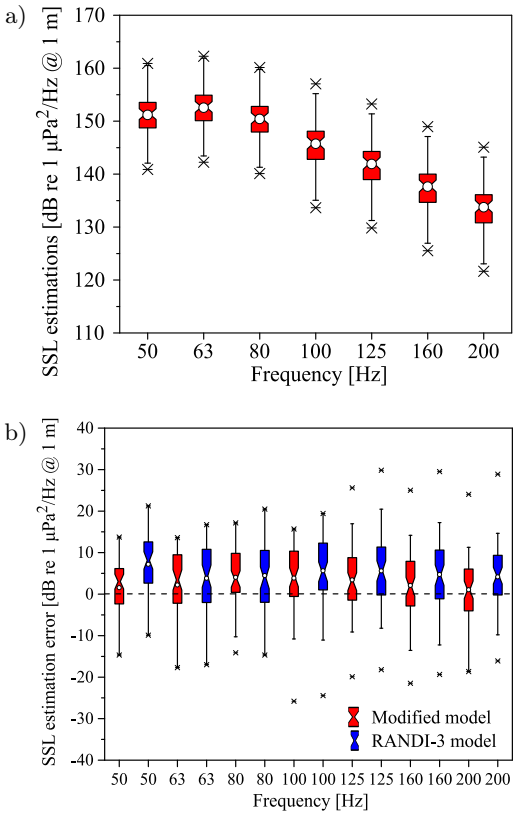

Fig. 7. a) SSL estimations of 57 merchant ships with modified model; b) comparison of estimation errors with RANDI-3 and modified model. The box notches are the medians; the bars are the 1st and 99th percentiles and markers are outliers.

d) the measurement cannot fulfil the requirements in ANSI S12.64 (2009) standard completely due to shallow waters.

However, from the viewpoint of the engineering application, the modified model is applicable and acceptable for us. It should be emphasized that the modified SSL model is only effective at frequencies from 50 Hz to 200 Hz in third-octave bands. Whether the modified model can be used in other groups of merchant ships needs more evidence from further measurements.

3. Shipping noise mapping in the waters of Zhoushan Archipelago

Our study site was located in the waters of Zhoushan Archipelago with many islands and reefs as shown in Fig. 8a. The acoustic observatory is marked as star symbol in Fig. 8a. As illustrated in Fig. 8b, the acoustic observatory was fastened with a rope, the other end of which was tied to a buoy set up with an Automatic Identification System (AIS). The interior of bottom-mounted hydrophone was equipped with a processor and memory, and the exterior of it was charged with a battery to fulfil the long-time data collection task underwater. The response of the hydrophone was −176 dB reμV/Pa and its sampling frequency was commonly set as 256 kHz. Each data file records 1-min radiated noise data. The experimental area can be characterized as a flat bottom with 24-m depth roughly. The sea floor is composed of a layer of clayey silt with 35 cm thickness and a half infinite layer of fine sand (Li, 1990). It should be noted that depth on the surface is taken as zero and the underwater part is taken as negative. The TLs were calculated with adiabatic normal modes theory, and the eigenvalues were precalculated using KRAKENC for each shipping noise source (Porter, 1990). The slopes near the island shores are very small, which makes the shipping noise decayed gradually when transmitting from the shallow water. Hence, the 3D refraction from the islands and reefs can be negligible when calculated, but for the ships transmitting from deeper water in the channel, there may be 3D refraction. Here, we adopted $N \times 2D$ calculation method by simply running the 2D models repeatedly along different bearings and combining these results to build-up a 3D acoustic field, which sacrificed the accuracy to some extent inevitably, but the computational load was much smaller for the $N \times 2D$

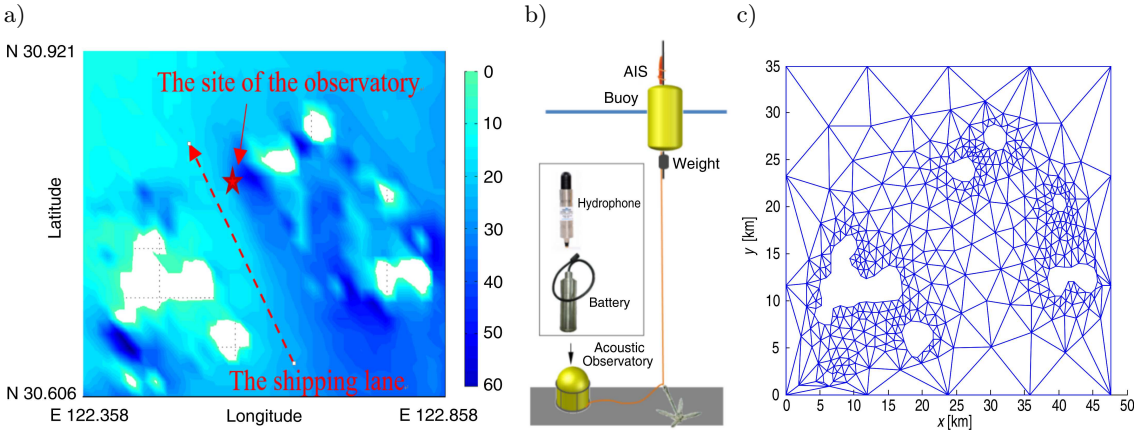

Fig. 8. Zhoushan Archipelago environment for 3D transmission loss calculation: a) bathymetry and position of the area, b) layout of the opportunistic acoustic observatory, c) triangulation of the area in a standard form by KRAKEN codes.

approximation. The environment was sampled at a number of different points in the xy-plane and modes were calculated at each of these points (Jensen *et al.*, 2010). Nodes were then generated to construct a triangulation of the environment in a standard form by KRAKEN codes, as shown in Fig. 8c (Peng *et al.*, 2018).

For the purpose of noise modelling, the AIS data samples within the study area were made available. The AIS data contains two parts of information. One is the positions (coordinate in xy-plane) of observed ships, and the other is the basic information of observed ships. The basic information contains the ship type, ship length L, tonnage T, shipping speed V, and draught d_S. On this basis, the SL can be estimated by the modified empirical model or the RANDI-3 model. Then, using KRAKENC, and combining the geoacoustic properties of continental shelf and slope environments, the noise mapping can be computed. This research process is shown in Fig. 9.

On the basis of the above study methodology, we chose the AIS samples observed at 11:50 on June 7, 2017 within the area shown in Table 2. The ships were limited to those with length greater than 40 m and speed greater than 7 kn. The basic information of chosen ships is listed in Table 2. The list contains ships that were present at the time and are taken from another data set rather than the 57 ships used to determine the empirical source levels.

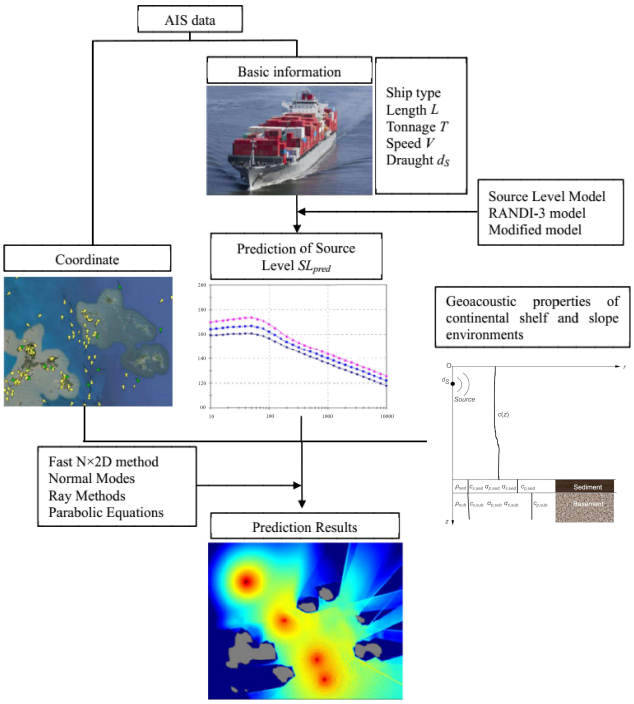

Fig. 9. Global flow chart of shipping noise prediction.

The SSLs of the 24 selected ships computed using the modified empirical SSL model combining the ship lengths and speeds presented in Table 3 are shown in Fig. 10a. From Table 3, longitudes and latitudes of the

Table 3. Information of observed ship in this area (@ 11:50 on June 7, 2017).

MMSI	Longitude [°]	Latitude [°]	Ship type	Length [m]	Draught [m]	Speed [kn]
100900000	122.3742	30.71448	cargo	50	3.5	10.2
412380070	122.5004	30.89791	tanker	138	5.6	11.5
412419750	122.5767	30.77090	cargo	121	8.2	10.2
412437030	122.6086	30.64278	cargo	107	5.5	8.8
412459950	122.5641	30.83468	cargo	128	3.6	8.9
412705460	122.6167	30.71280	cargo	97	3.8	9.5
412761450	122.6216	30.64639	cargo	97	3.8	8.8
412766790	122.3723	30.76263	tanker	82	4.6	9.9
412842000	122.5741	30.86664	cargo	190	5.9	12.0
413204070	122.6036	30.70907	cargo	96	5.6	8.6
413272340	122.5979	30.72653	cargo	97	6.0	9.5
413361940	122.5514	30.88592	cargo	118	4.5	9.8
413363380	122.3866	30.64860	cargo	135	4.5	11.0
413374760	122.5882	30.76231	cargo	97	5.5	9.1
413439061	122.4688	30.68612	cargo	60	4.2	9.5
413445540	122.6302	30.69032	tanker	122	7.0	11.4
413445890	122.5229	30.89836	cargo	190	6.0	12.8
413464910	122.5411	30.88266	cargo	96	5.8	7.7
413469000	122.5435	30.87242	cargo	96	5.5	7.8
413523530	122.5561	30.82118	cargo	92	5.0	8.8
413556090	122.4943	30.63142	cargo	131	6.1	10.4
413640000	122.5995	30.76873	cargo	124	7.0	7.5
538005698	122.6466	30.68688	cargo	179	5.5	13.7
900300003	122.5003	30.75330	fishing	40	3.5	9.4

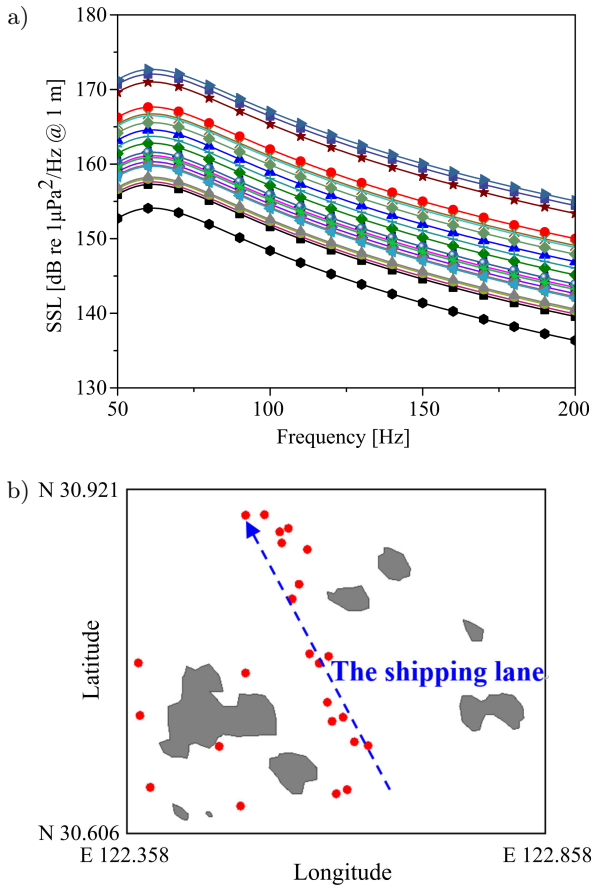

Fig. 10. a) Source level estimations of the 24 selected ships in this area; b) source level estimations of the selected ships in this area.

selected ships are plotted in Fig. 10b. Obviously, the distribution of ships is mainly along the channel from the south to the north among the islands.

By combining the source level estimations (see Fig. 10a) and the corresponding positions (Fig. 10b) with source depths which are set as two thirds of the ship draughts, the noise mapping at 10 m under the sea surface was obtained according to the energy superposition method, as shown in Fig. 11.

As illustrated in Fig. 11, for the low frequencies, such as 63 Hz, the propagation ranges of shipping noise are not further than that at higher frequencies. The reason for the low noise field to the north, and for the behavior at low frequencies is likely that the shallow water does not support modes, i.e. mode cut-off due to water depth and low frequency. Besides, from the noise mapping, the shielding effect of islands can be observed prominently. The propagation ranges in the north are not further than that in the south (see Fig. 10a), as the waters in the north are shallower.

To investigate the noise contribution of individual ship sources at the location of the acoustic observatory (marked as star symbol in Fig. 10a), the noise levels from all the ships are computed, as shown in Fig. 12. The observed ships were assigned their original bearings, shown by the lines from the observation point in Fig. 12. The length of each line represents the noise level of each corresponding ship, and the bearing of each line represents the bearing relationship between source and observed location (Breeding *et al.*, 1996).

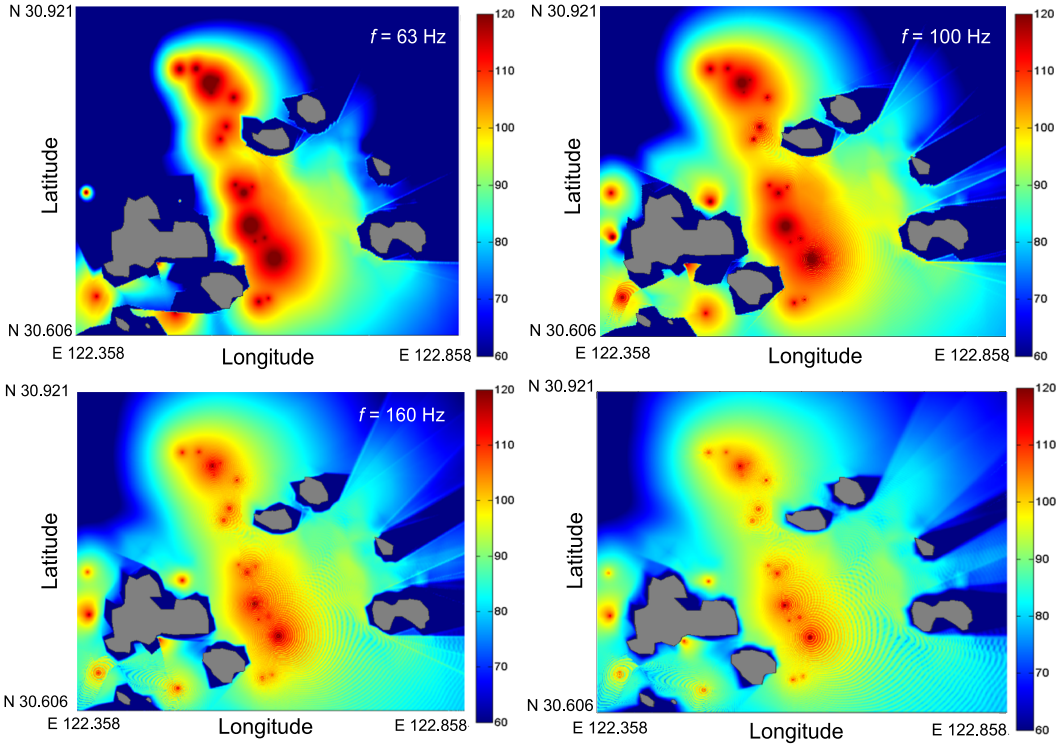

Fig. 11. Horizontal noise field produced by all observed ships with receiving depth of 10 m in the whole area.

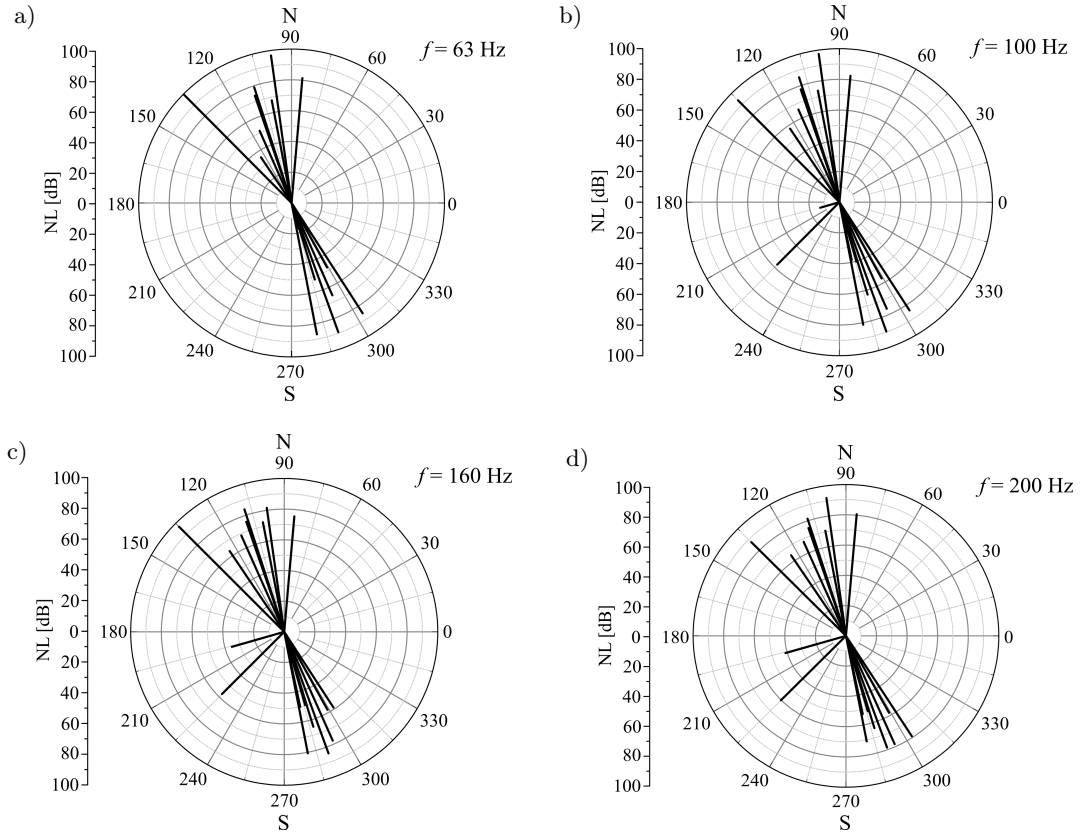

Fig. 12. Noise contribution from merchant ships at observed location with receiving depth of 10 m.

From Fig. 12, the noise contribution from ships at observed location is mainly concentrated along the direction from the northwest (90°~135°) to the southeast (270°~315°) due to the shielding effect of islands. Although the noise field is different at different frequencies, the noise contribution from the direction of 135° is the largest at all frequencies, and the largest level is as high as ~100 dB. Also, a number of ships were obviously found to be blocked from the receiver.

4. Summary and discussion

This paper presents two works made by us, observation and modelling on the shipping noise in shallow waters of the East China Sea. Some conclusions are made and listed as below:

1) Based on the shipping noise data measured in the East China Sea, we found that several classical empirical models (Urick model, Ross model, W&H model, and RANDI-3 model) are not accurate enough for some detailed ships, which have significant difference with the measured results. Especially for the frequencies below 100 Hz, the frequency dependency of source level is not monotonous and relatively complicated.
2) After analysing measured results, inspired by the RANDI-3 model, we tried to propose a modified SSL model for RANDI-3 model. The result shows that the modified SSL model has better estimation accuracy than RANDI-3 model in a certain range of ship length, speed and frequency. The median of the estimation error using this modified model with 0.89~3.49 is less than that using RANDI-3 model with 3.98~7.40 over the entire band.
3) Using the modified model and combining with the geoacoustic environment parameters, the noise field produced by shipping noise sources was present. The basic information of merchant ships was given by AIS data. The shipping noise source was modelled by the empirical SSL model. The propagation range depends on the frequency and is also influenced by the shielding effect of islands.
4) The noise contribution of individual source for a given observatory location shows that the noise contribution from ships at observed location is mainly influenced by the shielding effect of islands, which makes the noise contribution from ships at observed location mainly concentrated along the direction from the northwest (90°~135°) to the southeast (270°~315°).

Acknowledgements

This work was supported by the Foundation Strengthening Program Area Fund of Science and

Technology Commission of the Central Military Commission (No. 2020-JCJQ-JJ-228), Key Laboratory Fund of Underwater Measurement and Control Technology (6142407180205), Natural Science Foundation of Jiangsu Province (BK20200995), Scientific Research Start-Up Fund for Young Teachers of Jiangsu University of Science and Technology (1142931805) and the Institute of Acoustics of the Chinese Academy of Sciences (IOA, CAS). The first author would like to thank Prof. Weilin Tang for his suggestions. Finally, we would like to thank the anonymous reviewers for the insightful comments and helpful suggestions.

References

1. ANSI/ASA S12.64-2009 (2009), *Quantities and Procedures for Description and Measurement of Underwater Sound from Ships – Part 1: General Requirements.*
2. Audoly C. *et al.* (2017), Mitigation of underwater radiated noise related to shipping and its impact on marine life: a practical approach developed in the scope of AQUO project*, IEEE Journal of Oceanic Engineering*, **42**(2): 373–387, doi: 10.1109/JOE.2017.2673938.
3. Audoly C., Rizzuto E. (2015), AQUO: Achieve QUieter Oceans by shipping noise footprint reduction FP7-Collaborative project No 314227, WP 2: Noise Sources, Task T2.1, "Ship underwater radiated noise patterns", www.aquo.eu.
4. Breeding Jr. J.E., Pflug L.A., Bradley M., Walrod M.H. (1996), *Research Ambient Noise Directionality (RANDI) 3.1 Physics Description*, NRL Report, No. NRL/FR/7176–95-9628, Naval Research Laboratory, Stennis Space Center, MS.
5. Brooker A., Humphrey V. (2016), Measurement of radiated underwater noise from a small research vessel in shallow water, *Ocean Engineering*, **120**: 182–189, doi: 10.1016/j.oceaneng.2015.09.048.
6. Chen D. (1992), *Marine Atlas of Bohai Sea, Yellow Sea, East China Sea: Hydrology* [in Chinese], Beijing: China Ocean Press.
7. Colin M. *et al.* (2015), Definition and results of test cases for shipping sound maps, [in:] *Proceedings of IEEE-MTS OCEANS Conference*, Genova, Italy, May 18–21, pp. 1–19, doi: 10.1109/OCEANS-Genova.2015.7271461.
8. Erbe C., MacGillivray A., Williams R. (2012), Mapping cumulative noise from shipping to inform marine spatial planning, *The Journal of the Acoustical Society of America*, **132**(5): EL423–EL428, doi: 10.1121/1.4758779.
9. Folegot T. *et al.* (2015), Monitoring long term ocean noise in European waters, [in:] *Proceedings of IEEE-MTS Oceans Conference*, Genoa, Italy, May 18–21, 2015, pp. 1–7, doi: 10.1109/OCEANS-Genova.2015.7271394.
10. Hamilton E.L. (1980), Geoacoustic modeling of the sea floor, *The Journal of the Acoustical Society of America*, **68**(5): 1313–1340, doi: 10.1121/1.385100.
11. Hermannsen L., Beedholm K., Tougaard J., Madsen P.T. (2014), High frequency components of ship noise in shallow water with a discussion of implications for harbor porpoises (Phocoena phocoena), *The Journal of the Acoustical Society of America*, **136**(4): 1640–1653, doi: 10.1121/1.4893908.
12. Jensen F.B., Kuperman W.A., Porter M.B., Schmidt H. (2010), *Computational Ocean Acoustics*, Springer Science & Business Media.
13. Leissing T., Audoly C., Rousset C. (2014), Influence of ship radiated noise level directivity on the assessment of underwater noise maps, [in:] *Proceedings of 2nd International Conference and Exhibition on Underwater Acoustics*, June 22–27, 2014, Rhodes, Greece, pp. 1609–1614.
14. Li Q.X. (1990), *Marine Atlas of Bohai Sea, Yellow Sea, East China Sea: Geology and Geophysics* [in Chinese], China Ocean Press, Beijing, p. 13.
15. Mustonen M. *et al.* (2019), Spatial and temporal variability of ambient underwater sound in the Baltic Sea, *Scientific Reports*, **9**(1): 1–13, doi: 10.1038/s41598-019-48891-x.
16. National Research Council (2003), *Ocean Noise and Marine Mammals*, National Academies Press, Washington.
17. Peng Z., Wang B., Fan J. (2018), Assessment on source levels of merchant ships observed in the East China Sea, *Ocean Engineering*, **156**: 179–190, doi: 10.1016/j.oceaneng.2018.02.035.
18. Porter M.B. (1990), *The KRAKEN normal mode program.* SACLANT Undersea Research Centre technical report.
19. Robinson S.P. *et al.* (2011), *Measurement of underwater noise arising from marine aggregate dredging operations*, Marine Aggregate Levy Sustainability Fund MEPF report 09/P108.
20. Sertlek H.Ö., Binnerts B., Ainslie M.A. (2016), The effect of sound speed profile on shallow water shipping sound maps, *The Journal of the Acoustical Society of America*, **140**(1): EL84–EL88, doi: 10.1121/1.4954712.
21. Simard Y., Roy N., Gervaise C. (2016), Analysis and modeling of 255 source levels of merchant ships from an acoustic observatory along St. Lawrence Seaway, *The Journal of the Acoustical Society of America*, **140**(3): 2002–2018, doi: 10.1121/1.4962557.
22. Soares C., Zabel F., Jesus S.M. (2015), A shipping noise prediction tool, *OCEANS 2015 – Genova*, IEEE, pp. 1–7, doi: 10.1109/OCEANS-Genova.2015.7271539.